Inorg. Chem. **2002**, *41*, 3121–3127

Site-Selective EXAFS in Mixed-Valence Compounds Using High-Resolution Fluorescence Detection: A Study of Iron in Prussian Blue

Pieter Glatzel,[†] Lilian Jacquamet,[†,‡] Uwe Bergmann,[†,§] Frank M. F. de Groot,[||] and Stephen P. Cramer*[,†,§]

Department of Applied Science, University of California, Davis, California 95616, Lawrence Berkeley National Laboratory, Berkeley, California 94720, and Department of Chemistry, Utrecht University, 3584 CA Utrecht, The Netherlands

Received July 5, 2001

A quantitative analysis is presented for the site-selective Fe K-edge absorption spectra of Prussian Blue: $Fe_4[Fe(CN)_6]_3 \cdot xH_2O$ ($x = 14$–16). The site-selective spectra were recorded using high-resolution fluorescence detection of the Kβ emission from a polycrystalline sample. The Kβ fluorescence lines arising from the high-spin and low-spin sites are shifted in energy. Since the emission features partially overlap, fluorescence-detected absorption spectra using different emission energies represent different linear combinations of the pure high-spin and low-spin EXAFS. A numerical method was used to extract the individual site EXAFS spectra from the experimental data. The analysis yields a range of solutions. A unique solution can be obtained if homovalent model compounds are used to simulate the Kβ fluorescence emission from the two Fe sites in Prussian Blue. EXAFS analysis of the range of spectra obtained in the numerical method yields almost identical interatomic distances for the different spectra while the Debye–Waller factors vary considerably. The distances obtained in the EXAFS fit correspond to the crystallographic distances.

Introduction

In science as in life, heterogeneity is more the rule than the exception. For the spectroscopist seeking to characterize a complex system, one of the first tasks is therefore to assign particular spectral features to specific sites or components of a sample. One of the attractions of extended X-ray absorption fine structure (EXAFS) spectroscopy has been that every element has distinct X-ray absorption edges. One can therefore study each element separately with EXAFS. However, compounds and materials with the same element in different chemical forms present a problem for EXAFS spectroscopy.

Mixed-valence complexes and materials constitute an important field where improved EXAFS selectivity would be useful.[1] They are encountered in a variety of biological and chemical settings and have been studied extensively for their interesting properties. Biological examples include the 4-Mn cluster in the oxygen-evolving complex of photosystem II,[2] the 2-Fe cluster in methane monooxygenase,[3] and the binuclear Cu_A site in cytochrome oxidase.[4] In materials science, mixed-valence metals are important in copper oxide high-critical-temperature superconductors,[5] high-T_{Curie} Cr^{III}–Cr^{II} cyanide molecular magnets,[6] and magnetoresistive materials such as manganite perovskites.[7] In this paper we

* Author to whom correspondence should be addressed. E-mail: spcramer@ucdavis.edu.
[†] University of California.
[‡] Current address: European Synchrotron Research Facility, B.P. 220, 38043 Grenoble Cedex, France.
[§] Lawrence Berkeley National Laboratory.
[||] Utrecht University.

(1) *Mixed Valency Systems: Applications in Chemistry, Physics and Biology*; Prassides, K., Ed.; Kluwer Academic: Amsterdam, 1990; Vol. 343.
(2) (a) Manchanda, R.; Brudvig, G. W.; Crabtree, R. H. *Coord. Chem. Rev.* **1995**, *144*, 1−38. (b) Yachandra, V. K.; Derose, V. J.; Latimer, M. J.; Mukerji, I.; Sauer, K.; Klein, M. P. *Science* **1993**, *260*, 675−679.
(3) (a) Westerheide, L.; Pascaly, M.; Krebs, B. *Curr. Opin. Chem. Biol.* **2000**, *4*, 235−241. (b) Merkx, M.; Kopp, D. A.; Sazinsky, M. H.; Blazyk, J. L.; Muller, J.; Lippard, S. J. *Angew. Chem. Int. Ed.* **2001**, *40*, 2782−2807.
(4) Michel, H.; Behr, J.; Harrenga, A.; Kannt, A. *Annu. Rev. Biophys. Biomol. Struct.* **1998**, *27*, 329−356.
(5) Orenstein, J.; Millis, A. J. *Science* **2000**, *288*, 468−474.
(6) Mallah, T.; Thiebaut, S.; Verdauger, M.; Veillet, P. *Science* **1993**, *262*, 1554−1557.
(7) Raveau, B.; Maignan, A.; Martin, C.; Hervieu, M. *Chem. Mater.* **1998**, *10*, 2641−2652.

10.1021/ic010709m CCC: $22.00
Published on Web 05/21/2002

report a site-selective EXAFS study of the first mixed-valence compound ever synthesized: $Fe^{III}_4[Fe^{II}(CN)_6]_3 \cdot xH_2O$ ($x = 14-16$) or "Prussian Blue" (PB).[8]

EXAFS is an established spectroscopic tool for determining short-range structure in molecules and solids.[9] The X-ray absorption spectrum can be obtained directly from a transmission measurement, or indirectly by electron yield or fluorescence yield measurements.[10] Solid state detectors with ~200 eV resolution are commonly used in fluorescence-detected X-ray absorption spectroscopy. Spectra recorded in this manner are element specific, but they average over all species of an element in a sample.

X-ray fluorescence, like absorption, is sensitive to the chemical environment. However, the chemical shifts are generally small, and in the hard X-ray region a high-resolution crystal analyzer is needed to observe these effects.[11] If the fluorescence lines could be completely separated in an emission spectrum, then clean site-selective EXAFS spectra could be obtained by recording the fluorescence intensity at different fluorescence energies while scanning the incident X-ray energy. In practice, the fluorescence lines usually overlap. High-resolution fluorescence excitation spectra at different emission energies then represent different linear combinations of the "pure" EXAFS from individual species. In this paper, we show that, in favorable cases and with appropriate numerical analysis, it is still possible to obtain close approximations to the "pure" EXAFS signals.

Site-selective X-ray absorption spectra have been recorded before, using different techniques such as ion-desorption detection, luminescence detection, X-ray standing waves, or diffraction anomalous fine structure (DAFS).[12] Each of these methods has its own advantages and limitations. The technique presented in this paper is not restricted by sample preparation, although it does require a significant shift in the fluorescence emission energy of the element at the different chemical sites. Here we use the chemically sensitive Kβ main line emission that occurs when a vacancy in the 1s shell of an atom is filled by a 3p electron. The resulting

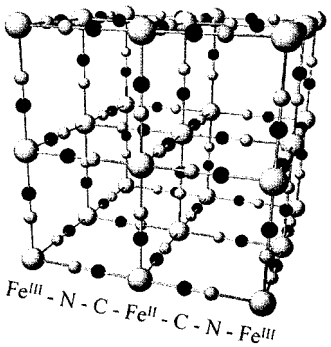

Figure 1. The unit cell of the PB crystal structure. Water molecules are omitted for simplicity. In bulk PB, every fourth $Fe^{II}(CN)_6$ group is missing and the nitrogen is replaced by an oxygen from water.

spectra reflect the multiplet splitting of the final states with a hole in the 3p shell: the unpaired electron spin in the 3p shell strongly interacts with the unpaired electron spins in the valence shells (essentially 3d) via the exchange interaction.[13] The 3p hole thus serves as a probe of the spin multiplicity, i.e. the net spin, localized at the emitting atom. The chemical sensitivity of the Kβ emission in 3d transition metals has been studied thoroughly, and Kβ fluorescence spectroscopy has been applied successfully to study oxidation and spin states of 3d metals in inorganic compounds and proteins.[13-15] Preliminary site-selective EXAFS data in mixed-valence Mn compounds were reported.[16] However, detailed evaluation of the spectra was limited by a poor signal-to-noise ratio in the fluorescence signal. Third-generation high-flux synchrotron radiation sources and a larger acceptance crystal array spectrometer have improved the data quality to allow for a thorough analysis of site-selective EXAFS.

The structure of $Fe_4(Fe(CN)_6)_3 \cdot 15H_2O$ was solved by Buser et al.[17] As illustrated in Figure 1, PB has a face-centered cubic lattice and contains two kinds of iron in different oxidation and spin states. The ferrous ion is coordinated by six carbons at 1.92 Å, followed by shells of six nitrogens at 3.05 Å and six ferric ions at 5.08 Å. The strong crystal field of the cyanide ligands yields a low-spin (LS) $(t_{2g})^6$ valence electron ground state configuration with zero net electron spin ($S = 0$). On the other hand, the occupancy of the $Fe^{II}(CN)_6$ site is 0.75 giving rise to a noninteger average composition of the ferric ion. An oxygen of a coordinated water replaces the nitrogen of the missing $Fe^{II}(CN)_6$ sites, and the coordination of the ferric ion can

(8) (a) *Miscellanea Berolinensia ad incrementum scientarium*; Berlin, 1710; p 377. (b) More accurately one has to distinguish between soluble and insoluble PB (see *Gmelins Handbuch der Anorganischen Chemie, Eisen B*; Verlag Chemie: Berlin, 1932; pp 670−723). In this paper PB always refers to the insoluble compound.

(9) Sayers, D. E.; Stern, E. A.; Lytle, F. W. *Phys. Rev. Lett.* **1971**, *27*, 1204−1206.

(10) Goulon, J.; Goulon-Ginet, C.; Cortes, R.; Dubois, J. M. *J. Phys.* **1982**, *43*, 539.

(11) Wang, X.; Grush, M. M.; Froeschner, A. G.; Cramer, S. P. *J. Synchrotron Radiat.* **1997**, *4*, 236−242.

(12) (a) Jaeger, R.; Stöhr, J. *Phys. Rev. Lett.* **1980**, *45*, 1870−1973. (b) Goulon, J.; Tola, P.; Brochon, J. C.; Lemonnier, M.; Dexpert-Ghys, J.; Guilard, R. In *EXAFS and Near Edge Structure III;* Hodgson, K. O., Hedman, B., Penner-Hahn, J. E., Eds.; Springer-Verlag: Berlin, 1984; pp 490−495. (c) Dexpert-Ghys, J.; Piriou, B.; Jacquetfrancillon, N.; Sombret, C. J. *Non-Cryst. Solids* **1990**, *125*, 117−128. (d) Yokoyama, T.; Takata, Y.; Yoshiki, M.; Ohta, T.; Funabashi, M.; Kitajima, C.; Kuroda, H. *Jpn. J. Appl. Phys.* **1989**, *28*, L1637−L1640. (e) Malgrange, C.; Ferret, D. *Nuclear Instrum. Methods Phys. Res. Sect. A* **1992**, *314*, 285−296. (f) Sorensen, L. B.; Cross, C. J.; Newville, O. M.; Ravel, B.; Rehr, J. J.; Stragier, H.; Bouldin, C. E.; Woicik, J. C. In *Resonant Anomalous X-Ray Scattering*; Materlik, G., Sparks, C. J., Fischer, K., Eds.; North-Holland: Amsterdam, 1994; pp 389−420. (g) Pickering, I. J.; Sansone, M.; Marsch, J.; George, G. N. *Jpn. J. Appl. Phys.* **1993**, *32*, 206−208.

(13) Meisel, A.; Leonhardt, G.; Szargan, R. In *X-Ray Spectra and Chemical Binding*; Schäfer, F. P., Goldanskii, V. I., Toennies, J. P., Eds.; Springer-Verlag: Berlin, 1989; Vol. 37.

(14) (a) Bergmann, U.; Grush, M. M.; Horne, C. R.; DeMarois, P.; Penner-Hahn, J. E.; Yocum, C. F.; Wright, D. W.; Dube, C. E.; Armstrong, W. H.; Christou, G.; Eppley, H. J.; Cramer, S. P. *J. Phys. Chem. B* **1998**, *102*, 8350−8352. (b) Peng, G.; Wang, X.; Randall, C. R.; Moore, J. A.; Cramer, S. P. *Appl. Phys. Lett.* **1994**, *65*, 2527−2529.

(15) Messinger, J.; Robblee, J. H.; Bergmann, U.; Fernandez, C.; Glatzel, P.; Visser, H.; Cinco, R. M.; McFarlane, K. L.; Bellacchio, E.; Pizarro, S. A.; Cramer, S. P.; Sauer, K.; Klein, M. P.; Yachandra, V. K. *J. Am. Chem. Soc.* **2001**, *123*, 7804−7820.

(16) Grush, M. M.; Christou, G.; Hämäläinen, K.; Cramer, S. P. *J. Am. Chem. Soc.* **1995**, *117*, 5895−5896.

(17) Buser, H. J.; Schwarzenbach, D.; Petter, W.; Ludi, A. *Inorg. Chem.* **1977**, *16*, 2704−2710.

vary from FeN_4O_2 to FeN_6, with an average composition of $FeN_{4.5}O_{1.5}$.[18] Thus, the ferric ion presents an averaged coordination shell constituted by 4.5 nitrogens at 2.03 Å and 1.5 oxygens at 2.14 Å and is surrounded by 4.5 carbons at 3.16 Å and 4.5 ferrous ions at 5.08 Å. EXAFS analysis (vide infra) will yield the result for the averaged ferric ion site. The Fe^{III} configuration is $(t_{2g})^3(e_g)^2$ high-spin (HS) with $S = {}^5/_2$. It is noteworthy that in fully hydrated PB the two irons, the carbon, and the nitrogen are arranged in a linear way. The bulk ratio high-spin Fe^{III} to low-spin Fe^{II} is 4:3. We neglect the uncoordinated water for the EXAFS analysis because of its large distance at 4.40 Å from the Fe ions and because it will not contribute to the multiple scattering (vide infra).

As models for the high-spin and low-spin sites in PB we have used Fe_2O_3 and $K_4Fe(CN)_6$, respectively.

Experimental Procedures

Sample Preparation and Characterization. Iron oxide (Fe_2O_3), potassium ferrocyanide ($K_4Fe(CN)_6$), and Prussian Blue ($Fe_4[Fe(CN)_6]_3 \cdot xH_2O$ ($x = 14-16$)) were used as received from Aldrich. In order to ensure identical crystal structures between the PB we used for the present study and the PB analyzed by Buser et al., we recorded the powder diffraction pattern of the Aldrich PB and found the structural parameters to agree within 0.4%.

Synchrotron Beamline. The fluorescence-detected XAS data were recorded on the BioCAT undulator beamline 18-ID at the Advanced Photon Source.[19] The energy of the incoming synchrotron beam was selected by means of a Si double-crystal monochromator with a (1,1,1) orientation. Higher harmonics were rejected by the focusing mirror. The incident beam was guarded by a 0.5 mm vertical by 1 mm horizontal slit in front of the samples. Using the fundamental undulator peak, the maximum incident flux was 10^{13} photons/s at 8 keV, as monitored by a nitrogen-filled ion chamber placed downstream of the guarding slit. However, in order to prevent detector saturation, the incident beam intensity was attenuated by Al foils that were inserted upstream of the guarding slit. The attenuation was selected depending on the detected fluorescence energy, and the incident flux on the sample surface was below 10^{12} photons/s for all fluorescence-detected absorption as well as the Kβ spectra. The incident X-ray monochromator energy bandwidth was ~1.2 eV at 8 keV energy.

Spectroscopy Measurements. The fluorescence emission from the samples was collected by a crystal array spectrometer.[20] The (6,2,0) Bragg reflection of six spherically bent Ge crystals arranged in a Rowland geometry was used. The analyzer crystals capture a solid angle of ≈0.013 sr. The diameter of each analyzer crystal is 1.75 in. A solid state (Ge) detector was placed at the common focus of the six crystals, and the entire emitted beam path was enclosed by a He-filled bag. The narrow energy bandwidth of the Ge detector (~200 eV at 7 keV) was used to window out unwanted X-ray photons and thus to improve the signal-to-background ratio. The ~0.8 eV analyzer bandwidth is determined by the intrinsic bandwidth of the crystals and geometrical contributions. Energy calibration was achieved by measuring the absolute angle of the Bragg reflection using optical tools. We estimate that the upper limit for the error of the absolute energy calibration is 1 eV. Possible changes of the energy calibration due to vertical movements of the synchrotron beam were checked by repeatedly measuring fluorescence from an Fe_2O_3 sample over the course of measurements; this error was found to be negligible. All spectra were recorded at room temperature. A total of 75 Kβ detected absorption scans were taken at three different fluorescence energies over an absorption scan range of 7.0−7.8 keV. The total counting time for each of the three fluorescence-detected absorption spectra is 75 min. The BioCAT beamline operates in continuous monochromator scan mode for absorption scans. Data are acquired "on the fly" during motor motion minimizing the dead time per scan. The monochromator energy calibration was constantly checked by recording the elastically scattered peak for each fluorescence-detected absorption scan. To minimize sample illumination a beam shutter was automatically inserted when no data were acquired during motor motions (monochromator or sample positioning). The incident X-ray beam position on the sample was changed after 15 min illumination time. As a measure of the sample integrity, we recorded Kβ spectra before and after a series of fluorescence-detected absorption scans for each illuminated position on the sample. No significant changes of the spectral features were observed, i.e., the Kβ spectra overlay within the statistical error. The $K\beta_{1,3}$ peak count rate was 30000 counts/s with negligible background, and considering the excellent signal-to-noise ratio, we state that no radiation damage occurred in the sample. The overall time needed for the present study was approximately 6 h.

Conventional, non-site-selective Fe K-edge XAS spectra for PB were recorded in transmission mode at room temperature on beamline 7-3 at the Stanford Synchrotron Radiation Laboratory (SSRL). Harmonic rejection was accomplished by detuning the monochromator crystals to 50% of maximum flux. Incident and transmitted beam intensities were measured using a nitrogen-filled ionization detector. The incident photon flux for the transmission experiment was 10^{10} photons/s.

In order to minimize fluorescence "saturation" and transmission "leakage" artifacts,[10] the samples for both experiments were made optically thin by diluting the pure sample with boron nitride.

EXAFS Extraction. The EXAFS signal was extracted from the raw excitation spectra using the previously described SEDEM package.[21] EXAFS spectra were k^3 weighted, Fourier-filtered between ca. 1.0 and 5.0 Å, and then back-transformed before the fitting procedure.

EXAFS Simulations. Ab initio calculations were performed with the FEFF 7.02 code[22] for both low-spin ferrous ion and high-spin ferric ion as the X-ray absorber. The initial calculations were done using the PB crystal structure of the fully hydrated compound.[17] For each shell, only the path with the highest probability was kept. The corresponding ab initio parameters (backscattering amplitude, total phase shift of the absorber−scatterer pairs, and mean free paths) were then introduced into the SEDEM fit program. For both sites we used a model with only three shells. Backscattering amplitude, phase shifts, and mean free paths for single paths (Fe^{II}−C or Fe^{III}−N) were used to fit the first-shell interaction. Because of the linear geometry, for the second and third shells, the strengths of multiple scattering interactions are stronger than the single

(18) Herren, F.; Fischer, P.; Ludi, A.; Hälg, W. *Inorg. Chem.* **1980**, *19*, 956−959.
(19) Bunker, G. B.; Irving, T.; Black, E.; Zhang, K.; Fischetti, R.; Wang, S.; Stepanov, S. *AIP Conf. Proc.* **1997**, *417*, 16.
(20) Bergmann, U.; Cramer, S. P. *Proc. SPIE—Int. Soc. Opt. Eng.* **1998**, *3448*, 198−209.
(21) (a) Adrait, A.; Jacquamet, L.; Le Pape, L.; de Peredo, A. G.; Aberdam, D.; Hazemann, J. L.; Latour, J. M.; Michaud-Soret, I. *Biochemistry* **1999**, *38*, 6248. (b) Jacquamet, L.; Dole, F.; Jeandey, C.; Oddou, J. L.; Perret, E.; Le Pape, L.; Aberdam, D.; Hazemann, J. L.; Michaud-Soret, I.; Latour, J. M. *J. Am. Chem. Soc.* **2000**, *122*, 394.
(22) Zabinsky, S. I.; Rehr, J. J.; Ankudinov, A.; Albers, R. C.; Eller, M. J. *Phys. Rev. B* **1995**, *52*, 2995−3009.

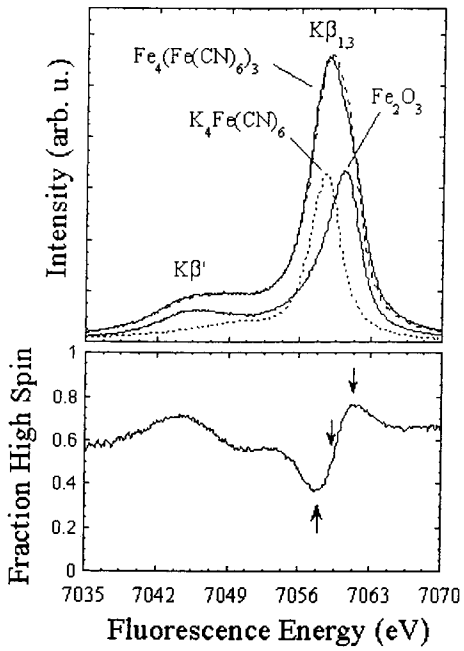

Figure 2. Upper panel, lower curves: Kβ spectra of Fe_2O_3 (solid line) and $K_4Fe(CN)_6$ (dotted line). The Fe_2O_3 and $K_4Fe(CN)_6$ spectra were normalized so that the ratio of the integrated intensities is 4:3, respectively, as is expected for the ratio high-spin Fe:low-spin Fe in PB. Upper panel, upper curves: $Fe_4[Fe(CN)_6]_3$ spectrum (solid line) vs normalized sum of Fe_2O_3 and $K_4Fe(CN)_6$ spectra (dashed line). Lower panel: Estimated fraction of signal arising from high-spin Fe^{III} component in the PB spectrum vs fluorescence energy, using Fe_2O_3 and $K_4Fe(CN)_6$ as models. The arrows indicate the fluorescence energies where site-selective absorption spectra were taken.

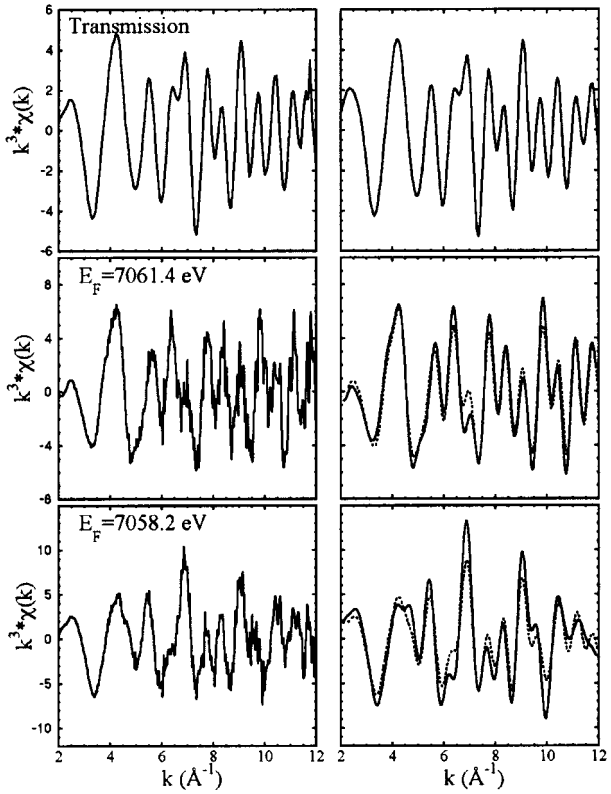

Figure 3. Left: Experimental *k*-space EXAFS spectra. Top to bottom: transmission mode; Kβ-detected at $E_F = 7061.4$ eV; Kβ-detected at $E_F = 7058.2$ eV. Right: Fourier-filtered experimental spectra (dotted lines) compared to the deduced "pure" site-selective EXAFS spectra obtained in the least-squares fit (solid lines). We show the deduced spectra that give the best EXAFS fit index and the smallest σ^2 values of the range given in Table 1. The spectrum taken at $E_F = 7061.4$ eV is compared to the deduced high-spin EXAFS, and the spectrum taken at $E_F = 7058.2$ eV is compared to the deduced low-spin EXAFS.

scattering components. Thus, for the second shell ($Fe^{II}-N$ or $Fe^{III}-C$) and the third shell ($Fe^{II}-Fe^{III}$ or $Fe^{III}-Fe^{II}$), backscattering amplitude, phase shifts, and mean free path of multiple paths were used to fit data.

Results

Kβ Spectra. The Kβ spectrum of Fe in PB is shown in Figure 2. The sharp line at high fluorescence energy is labeled K$\beta_{1,3}$, and the broader structure at lower energies Kβ'. The Kβ spectral features are broadened by contributions from the 1s and 3p core hole lifetimes and by other multiplet and spin−orbit splittings.[13,23,24] The analyzer bandwidth of ~0.8 eV is much smaller than the observed line width of 3−4 eV, and therefore it has only a negligible effect on the line broadening. The incident energy was set well above the Fe K-edge to record the Kβ spectra, and the monochromator energy bandwidth does not influence the Kβ spectral shape.

We used Fe_2O_3 and $K_4Fe(CN)_6$ as model compounds to help interpret the PB Kβ emission (Figure 2). A 1.9 eV shift toward lower fluorescence energies is observed for the K$\beta_{1,3}$ peak between high-spin Fe^{III} and low-spin Fe^{II}. Furthermore, the high-spin spectrum is split into a K$\beta_{1,3}$ peak and a lower energy Kβ' feature. This splitting comes primarily from the strong exchange interaction between partially filled 3p and 3d shells, i.e., the final states represented by the two lines differ with respect to the orientation of the 3p hole spin relative to the unpaired spins in the 3d shell. This explains why the splitting is essentially nonexistent in the low-spin $K_4Fe(CN)_6$ spectrum.

From the Kβ spectra of the two model compounds we obtained an approximate curve for the fractional contribution of high-spin Fe^{III} to the total PB Kβ spectrum at different fluorescence energies (Figure 2). We see that the high-energy side of the PB K$\beta_{1,3}$ line is due mainly to high-spin Fe^{III}, while the low-energy side reflects mostly the low-spin Fe^{II} contribution. The normalized sum of the two model compound spectra is compared to the PB spectrum in Figure 2. The satisfactory agreement gives us confidence in the predicted high-spin and low-spin contributions.

We used this information as a guide to determine favorable fluorescence energies: points with good high-spin:low-spin contrast. Three fluorescence-detected EXAFS spectra were taken at the fluorescence energies with the lowest (7058.2 eV, 38.0% HS), intermediate (7059.8 eV, 59.8% HS), and highest (7061.4 eV, 76.1% HS) estimated high-spin:low-spin ratios, as indicated in Figure 2. In addition, a non-site-selective absorption spectrum was recorded in transmission mode. The *k*-space EXAFS detected in transmission mode as well as the fluorescence-detected spectra with the highest and lowest high-spin fractions are shown in Figure 3.

(23) Krause, M. O.; Oliver, J. H. *J. Phys. Chem. Ref. Data* **1979**, *8*, 329−337.
(24) Glatzel, P.; Bergmann, U.; de Groot, F. M. F.; Cramer, S. P. *Phys. Rev. B* **2001**, *6404*, 5109.

Site-Selective EXAFS. The three Kβ-detected EXAFS spectra do not show the true EXAFS from one specific site because they contain admixtures from both Fe species in PB. It is therefore necessary to extract the actual EXAFS corresponding to the individual sites from the experimental spectra by a numerical procedure. We assume that each experimental spectrum (S_i^{exp}) can be described as a linear combination of the pure low-spin (S^{LS}) and pure high-spin (S^{HS}) absorption spectrum:

$$S_i^{exp} = c_i^{LS} S^{LS} + c_i^{HS} S^{HS}$$

This implies that the fluorescence-detected absorption spectra solely differ by their high-spin to low-spin ratio and that all other final state dependencies can be neglected, i.e., the partial fluorescence yield is proportional to the absorption cross section. For EXAFS, this assumption holds to sufficient accuracy, while for the XANES (X-ray absorption near edge structure) region where resonant excitations dominate, the final state term dependency has to be taken into account.

Using the model compounds, the coefficients c_i can be obtained from the high-spin:low-spin curve shown in Figure 2. If we use only the Kβ-detected absorption spectra with the highest and the lowest fraction high-spin, i.e., two experimental spectra, the system can be solved for S^{HS} and S^{LS} by taking the inverse of the 2×2 coefficient matrix. We will discuss this solution below. It is, however, not clear how well the model compounds represent the two sites in PB. We therefore chose to deduce the coefficients c_i in a least-squares fit independent of the model compounds using the Fourier-filtered EXAFS spectra of all three fluorescence-detected spectra as well as of the transmission spectrum. The transmission spectrum was included both because of the good signal-to-noise ratio and because it imposes a constraint on the coefficients c_i: the high-spin:low-spin ratio is 4:3 for this spectrum. The inclusion of the transmission spectrum does not limit the technique presented here because a non-site-selective absorption spectrum with a known ratio of the contributions from the different sites can always be obtained either in transmission mode or by using conventional fluorescence-detected absorption spectroscopy. The mathematical details of the fitting procedure are described in the Appendix. The outlined fitting procedure does not use any information from model compounds or crystallographic data. One parameter therefore remains undetermined in the fitting procedure as is described in the Appendix. Once a value for this parameter is chosen, the coefficients c_i and the high-spin and low-spin EXAFS spectra are uniquely determined. A range of "mathematical" EXAFS spectra is thus obtained each of which being an equally good result of the least-squares fit. This range of solutions includes the true, "physical" EXAFS spectra of the low-spin and the high-spin site. However, additional information about the compound under consideration is necessary in order to limit the range of mathematical solutions. In the following section, it is described how limits to the range of the undetermined parameter can be set in the case of PB.

EXAFS Analysis. EXAFS analyses were performed for the range of solutions resulting from the numerical procedure performed on the experimental spectra, and the distances as well as the σ^2 values were determined while the number of neighbors was held to their chemical value. We find that the distances hardly differ for the different solutions while the σ^2 values strongly vary and become unphysical outside a certain limit of the open parameter in the numerical deduction. Thus, solutions with unphysical σ^2 values can be easily ruled out. Alternatively, one can use the standard deviation or fit index[21] of the EXAFS analysis as a criterion to limit the range of solutions. We find that the best fits (i.e., with the smallest standard deviation or fit index) give physical σ^2 values. Table 1 summarizes the equivalent best fits with the corresponding set of distances and σ^2 values. The crystallographic distances are well reproduced, and the σ^2 values are within physical limits.

The Fourier-filtered *k*-space EXAFS of the experimental spectra with the highest and lowest fraction of high spin are compared in Figure 3 to the numerically deduced high-spin and low-spin EXAFS that yield the best fits with smallest σ^2 values in the EXAFS analysis as given in Table 1. Figure 4 shows the same deduced high-spin and low-spin EXAFS together with the EXAFS fits as well as the Fourier transforms of the deduced EXAFS with the corresponding

Table 1. Selected Curve-Fitting Results of Deduced High-Spin and Low-Spin Site EXAFS Spectra Together with the Crystallographic Distances[a]

Fe site in Prussian Blue	shell	type of neighbors	*R* (Å)	σ^2 (10^{-3} Å^2)	crystallographic distances (Å)
low-spin Fe^{II}	1	6 C	1.90−1.92	4.8−7.7	1.92
	2	6 N	3.02−3.04	3.4−4.9	3.05
	3	6 Fe	5.05−5.06	3.5−3.8	5.08
high-spin Fe^{III}	1	4.5 N/1.5 O	2.05−2.06	7.4−10.2	2.03/2.14
	2	4.5 C	3.18−3.19	4.3−5.6	3.16
	3	4.5 Fe	5.10	1.6−1.9	5.08

[a] A range of solutions is given for the distances and the σ^2 values obtained from the equivalent best fits to the deduced site-selective EXAFS.

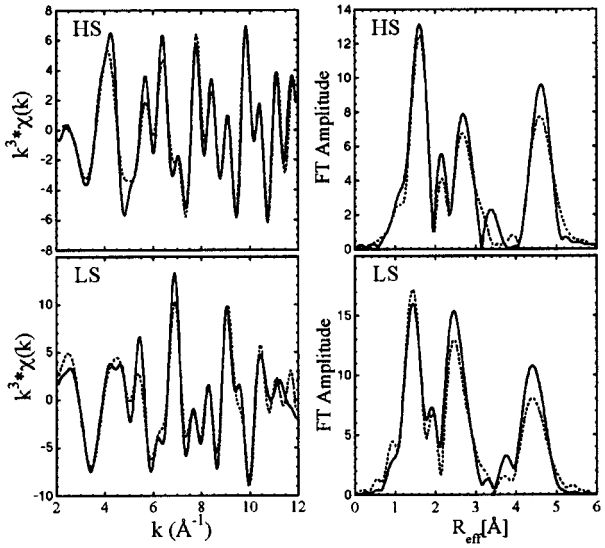

Figure 4. Left: Deduced site-selective EXAFS spectra (solid lines) for the high-spin (top) and low-spin (bottom) site in PB with the corresponding EXAFS fits (dotted lines). Right: Fourier transforms of the deduced EXAFS data (solid lines) with the corresponding fits (dotted lines).

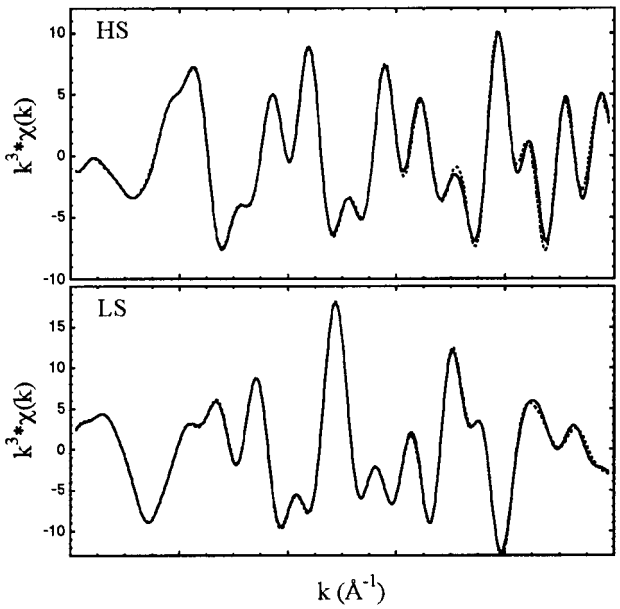

Figure 5. Comparison of deduced site-selective EXAFS data as obtained from the model compounds (solid lines) with one of the results of the numerical method that yields similar high-spin:low-spin ratios (dotted lines).

fits. The $Fe^{III}-O$ distance of 2.14 Å is longer than the $Fe^{III}-N$ distance of 2.03 Å. As a consequence, at a 10 $Å^{-1}$ space range, the oxygen shell is not discriminated from the nitrogen shell. For the other shells, scattering from oxygen will be negligible compared to the strong multiple scattering present. So, water oxygen atoms do not contribute significantly to the overall EXAFS.

Discussion. The technique presented here to obtain site-selective EXAFS in mixed-valence compounds has the advantage of being potentially applicable to any type of sample that can be measured in conventional fluorescence-detected absorption spectroscopy. However, the experimental spectra do not show the pure site-selective EXAFS. They only differ in the ratio of contributions from the different sites. Using a numerical procedure to deduce the pure EXAFS from the experimental spectra we obtain the crystallographic distances and a set of physical σ^2 values for each Fe site. The method appears to be consistent because the EXAFS simulations with the crystallographic distances and physical σ^2 values yield the best fit to the deduced site-selective spectra. As another check of our numerical method, we compare in Figure 5 the site-selective EXAFS extracted using the ratios given by the model compounds to the deduced site-selective EXAFS obtained in the least-squares fit. For the latter, we show a solution that gives high-spin: low-spin ratios similar to the values derived from the model compounds. The spectra are almost identical. The range of solutions obtained in the numerical method therefore includes the EXAFS spectra that are derived from the model compounds. The σ^2 values for this solution are 2.3, 1.9, and 3.0×10^{-3} $Å^2$ for the first, second, and third shell of the low-spin Fe^{II}, respectively. The corresponding values for high-spin Fe^{III} are 2.9, 2.4, and 1.2×10^{-3} $Å^2$. However, the fit index for the EXAFS analysis of the spectra shown in Figure 5 is not the best possible. We achieve better EXAFS fits for solutions where we use different values for the fraction of signal arising from high-spin Fe. The EXAFS spectra that are shown in Figure 4 give the best possible fit index and yield 25.5% (E_F = 7058.2 eV), 60.5% (E_F = 7059.8 eV), and 89.3% (E_F = 7061.4 eV) for the fraction of signal arising from high-spin Fe^{III}. These values imply that the K$\beta_{1,3}$ lines from the different sites in PB are actually better separated than the model compounds suggest (38.0%, 59.8%, and 76.1% for the fraction of signal arising from high-spin Fe^{III}). One possible explanation would be that the K$\beta_{1,3}$ line from Fe_2O_3 is broader than the K$\beta_{1,3}$ line from high-spin Fe^{III} in PB.

High-spin vs low-spin Fe in PB has a relatively large fluorescence shift and is clearly a favorable case. The comparison in Figure 3 between the experimental and the deduced EXAFS shows only little differences in particular for the high-spin site, indicating that we chose optimal fluorescence energies to record site-selective spectra. That was possible because we could use model compounds. Good models are not always available, and most mixed-valence compounds will show smaller K$\beta_{1,3}$ fluorescence energy shifts. Hence, it is fair to ask how general this technique can be and how large a shift in fluorescence energy is necessary to extract the pure site-selective EXAFS. We note that a change in formal oxidation state, i.e., a change in net spin of $\Delta S = {}^1/_2$, results in a shift in the Kβ fluorescence energy of 0.3−0.6 eV for most early transition metal compounds with weak electron correlation. If no good model compounds exist and for small shifts, one can record Kβ-detected absorption spectra at more than three fluorescence energies and thus improve the numerical extraction procedure. Here we note that the overall data-taking time of 6 h needed for the present study could be reduced considerably if a faster detector were available.

Potentially useful Kβ shifts generally exist between a metal and its oxidized forms; hence catalysis is one potential application area. Light elements such as carbon also have relatively large shifts between different chemical forms. Finally, we note that valence → core fluorescence spectra (K$\beta_{2,5}$ and Kβ'' lines) that are a factor of 50−100 weaker than the K$\beta_{1,3}$ lines have even larger chemical shifts. Using these spectral features for site-selective EXAFS involves some experimental difficulties (e.g., larger background mainly due to Compton scattering). But the difficulties can be overcome and eventually it will be possible to take advantage of these weaker features for site-selective spectroscopy.

Conclusion. We have presented a quantitative analysis of Kβ-detected, site-selective EXAFS spectra in Prussian Blue**.** Our study shows that high-resolution fluorescence-detected absorption spectroscopy is a viable approach to record site-selective EXAFS. The limitation of this technique arises from possibly insufficient separation of the fluorescence lines from the two sites. Future studies on mixed-valence compounds will have to show how generally applicable this method actually is.

Acknowledgment. Use of the Advanced Photon Source was supported by the U.S. Department of Energy, Basic Energy Sciences, Office of Science, under Contract No. W-31-109-ENG-38. BioCAT is a National Institutes of Health supported Research Center RR-08630. We thank Dr. Artur Braun for recording the powder diffraction pattern and Plamen Koev for advice on the numerical procedure. This work was support by the National Institutes of Health, Grants GM-44380, and the Department of Energy, Office of Biological and Environmental Research.

Appendix

To deduce the EXAFS spectra at the high-spin and low-spin site we write the spectra in a matrix equation $\mathbf{AX} = \mathbf{Y}$, where $\mathbf{A}$ represents the 4×2 matrix for the coefficients c_i, $\mathbf{X}$ the $2 \times n$ matrix for the true Fe EXAFS at the two sites, and $\mathbf{Y}$ the $4 \times n$ matrix containing the experimental spectra (n being the number of data points):

$$\begin{pmatrix} c_a^{LS} & c_a^{HS} \\ c_b^{LS} & c_b^{HS} \\ c_c^{LS} & c_c^{HS} \\ c_d^{LS} & c_d^{HS} \end{pmatrix} \begin{pmatrix} l_1 & l_2 & \dots & l_n \\ h_1 & h_2 & \dots & h_n \end{pmatrix} = \begin{pmatrix} a_1 & a_2 & \dots & a_n \\ b_1 & b_2 & \dots & b_n \\ c_1 & c_2 & \dots & c_n \\ d_1 & d_2 & \dots & d_n \end{pmatrix}$$

The pure site-selective EXAFS spectra are written in the rows with the elements l_j and h_j. This is an overdetermined system with $4 \times 2 + 2 \times n$ unknown and $4 \times n$ equations. It contains, however, experimental data with statistical errors and therefore has to be solved in a least-squares fit. In terms of linear algebra we are looking for the best rank-2 approximation to a rank-4 matrix.[25] This means that we aim to minimize the two-norm, which is a least-squares fit, of a system $||\mathbf{A'X'} - \mathbf{Y}||$, where $\mathbf{A'}$ and $\mathbf{X'}$ are any 4×2 and $2 \times n$ matrixes that minimize the two-norm but are not necessarily the physical solution $\mathbf{A}$ and $\mathbf{X}$ of our problem. In mathematical terms we can say that there is a space spanned by combinations of 4×2 and $2 \times n$ matrixes that minimizes the two-norm. We thus do not obtain a unique solution, and we have to pick the physical solutions from this space of mathematical solutions. The matrixes $\mathbf{A'}$ and $\mathbf{X'}$ are found using the principle of single value decomposition in linear algebra. We did this using the program Matlab. In the next step we write $\mathbf{AX} = (\mathbf{A'M})(\mathbf{M}^{-1}\mathbf{X'})$ where $\mathbf{A}$ and $\mathbf{X}$ are the physical solutions we are looking for. We note that there is one and only one matrix $\mathbf{X}$ for each coefficient matrix $\mathbf{A}$ that defines the fraction of signal arising from high spin for the experimental spectra. $\mathbf{AX}$ still minimizes the two-norm of $||\mathbf{A'X'} - \mathbf{Y}||$, i.e., it is a solution of the least-squares fit, because $\mathbf{MM}^{-1} = \mathbf{E}$ where $\mathbf{E}$ is the identity matrix. $\mathbf{M}$ is a 2×2 matrix. In order to determine $\mathbf{M}$ we impose the constraint on all coefficients c_i that they are positive and that their sum for each experimental spectrum is 1. This is justified by the fact that all EXAFS spectra used for the least-squares fit are normalized to each other by using the atomic cross section. We thus write

$$\mathbf{A} = \begin{pmatrix} c_a^{LS} & 1 - c_a^{LS} \\ c_b^{LS} & 1 - c_b^{LS} \\ c_c^{LS} & 1 - c_c^{LS} \\ c_d^{LS} & 1 - c_d^{LS} \end{pmatrix} = \mathbf{A'M} = \begin{pmatrix} c'^{LS}_a & c'^{HS}_a \\ c'^{LS}_b & c'^{HS}_b \\ c'^{LS}_c & c'^{HS}_c \\ c'^{LS}_d & c'^{HS}_d \end{pmatrix} \begin{pmatrix} m_1 & m_2 \\ m_3 & m_4 \end{pmatrix}$$

This system of equations can be rewritten as

$$\begin{pmatrix} 1 \\ 1 \\ 1 \\ 1 \end{pmatrix} = \begin{pmatrix} c'^{LS}_a & c'^{HS}_a \\ c'^{LS}_b & c'^{HS}_b \\ c'^{LS}_c & c'^{HS}_c \\ c'^{LS}_d & c'^{HS}_d \end{pmatrix} \begin{pmatrix} m_1 + m_2 \\ m_3 + m_4 \end{pmatrix}$$

and solved for $m_1 + m_2 = s_1$ and $m_3 + m_4 = s_2$ again in a least-squares fit (using Matlab) giving two equations. A third equation is obtained from the known high-spin:low-spin ratio for the transmission spectrum. We leave m_4 as the open parameter and obtain for the other parameters $m_3 = s_2 - m_4$, $m_2 = {}^4/_7(s_1 + s_2 c'^{HS}_d/c'^{LS}_d) - m_4 c'^{HS}_d/c'^{LS}_d$ and $m_1 = s_1 - m_2$. The constraint that all coefficients c_i are positive sets one limit to the range for the open parameter m_4. Table 1 shows the results for m_4 varying between 0.3 and 0.7.

IC010709M

(25) Demmel, J. W. *Applied numerical linear algebra*; Society for Industrial and Applied Mathematics: Philadelphia, 1997.